Single spin detection and noise spectroscopy

Z. Nussinov [a], Jian-Xin Zhu [a], A. V. Balatsky [a], M. F. Crommie [b,c], and Y. Manassen [d]

[a] Theoretical Division, Los Alamos National Laboratory, NM 87544;
[b] Department of Physics, University of California, Berkeley, CA 94720 ;
[c] Materials Sciences Division, Lawrence Berkeley Laboratory, CA 94720 ;
[d] Department of Physics and Ilan Katz Center For Nanometer Scale Science and Technology, Ben Gurion University, Beer Sheva, 84105 Israel

ABSTRACT

We discuss non-trivial effects which emerge when a single spin is embedded in various (normal and Josephson) junctions and discuss a new experimental technique to probe single spin dynamics. We show that current may be influenced by the presence of a single spin and the converse. New spin nutations in a Josephson junction are predicted. We discuss a new general exerimental technique to probe single spin dynamics via noise spectroscopy- by carefully monitoring the current noise, important information can be extracted regarding a single spin motion.

Keywords: spin precessing, current modulation and fluctuations

1. INTRODUCTION

There has been intensified interest in the electronic transport through atomic impurities or quantum dots in condensed matter physics. The novel features arising from the quantization of both the electronic spectrum and the electronic charge on these impurities have been well studied. More recently, the behavior of a single magnetic spin has also received much attention. No fundamental principle precludes the measurement of a single spin, and therefore the capability to make such a measurement depends on our ability to develop a detection method of sufficient spatial and temporal resolution. The standard electron spin detection technique- electron spin resonance- is limited to a macroscopic number ($\geq 10^{10}$) of electron spins.[1] Recent experiments employing spin polarized STM (scanning tunneling microscope)[2] open new possibilities of investigation of magnetic systems at spatial resolutions of the atomic scale. Single spin detection and manipulation may play a major role in spintronics and quantum information processing. In spintronics, spins can be used as elementary information storage units.[3,4] In the realm of quantum computing,[5,6] several architecture proposals rely crucially on the ability to manipulate and detect single spins. Thus far, the possibility of a single spin observation is a challenging issue. The state-of-the-art magnetic resonance force microscopy has recently achieved the resolution of about 100 fully polarized electron spins.[7] The atomic resolution of the STM can provide an alternative technique for the single spin detection .[8,9] In this paper, we address various spintronic systems in which a magnetic spin is weakly coupled to two leads. The leads may be two normal conductors, two superconductors (a Josephson junction) or may represent an STM tip and a non-magnetic surface. The outline is as follows: In Section 2, we illustrate how the current flowing in a normal junction immersed in a weak magnetic field may be modulated by a single spin, thus allowing single spin detection. In section 3, we illustrate the converse- we show that rather novel single spin cluster dynamics can emerge when spins are embedded within Josephson junctions. We provide explicit predictions for this new effect and suggest its detection. In section 4 we introduce a new experimental technique for monitoring the dynamics of a single spin. Here, the two leads of previous sections refer to a polarized STM tip and a normal non-magnetic surface. We propose that the noise in the current may allow to directly monitor a fluctuating single spin state.

Further author information:
Z. Nussinov: Email: zohar@viking.lanl.gov, Telephone: 1 505 665 9792
Jian-Xin Zhu: E-mail: jxzhu@viking.lanl.gov, Telephone: 1 505 667 2363
A. V. Balatsky: E-mail: avb@viking.lanl.gov, Telephone: 1 505 665 0077
M. F. Crommie: E-mail: crommie@socrates.Berkeley.EDU, Telephone: 1 510 642-9392
Y. Manassen: E-mail: manassen@bgumail.bgu.ac.il Telephone: +972-8-647-2153

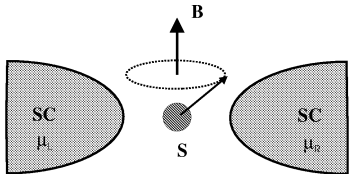

Figure 1. Magnetic spin coupled to two leads.

2. MODULATION OF TUNNELING CURRENT

In this section, we analyze the modulation of tunneling current between two metallic leads when an intervening single spin is introduced. We predict the existence of an oscillation mode whose frequency is twice the Larmor frequency. The model system under consideration is illustrated in Fig. 1.

In the presence of a magnetic field, the spin precesses around the field direction. We assume that there are no electron-electron interaction and spin-orbit interactions within the metallic leads. We model the spin and its leads by the Hamiltonian:

$$\mathcal{H} = \sum_{k\in(L,R),\sigma} \epsilon_{k\sigma} c^\dagger_{k\sigma} c_{k\sigma} + J \sum_{\sigma,\sigma'} d^\dagger_\sigma \Omega_{\sigma\sigma'} d_{\sigma'} + \sum_{k\in(L,R),\sigma;\sigma'} (V_{k\sigma,\sigma'} c^\dagger_{k\sigma} d_{\sigma'} + \text{H.c.}) \,. \tag{1}$$

Here $c^\dagger_{k\sigma}$ ($c_{k\sigma}$) creates (destroys) an electron with momentum k and spin σ in either the left (L) or the right (R) lead, and $d^\dagger_\sigma$ (d_σ) is the creation (annihilation) operator of the single electron with spin σ at the magnetic spin site. The quantity $\epsilon_{k\sigma}$ are the single particle energies of conduction electrons in the two leads. The electrons on the spin impurity site is connected to those in the two leads with the tunneling matrix elements $V_{k\sigma,\sigma'}$. The single electron on the impurity site is coupled to the local spin through a direct exchange interaction of strength J. The form of the coupling matrix $\hat{\Omega}$ in Eq. (1) will be discussed below. Since the Zeeman coupling of the electrons on the impurity site to the external magnetic field is usually very small compared with the exchange coupling to the local spin, this interaction term has been neglected. The local magnetic spin $\mathbf{S}$ is defined in a three-dimensional spin space. In an external magnetic field $\mathbf{B}$, a torque will act on the magnetic moment μ of amount $\mu \times \mathbf{B}$, where $\mu = \gamma \mathbf{S}$ with γ the gyromagnetic ratio. The equation of motion of the local spin is given by $\frac{d\mu}{dt} = \mu \times (\gamma \mathbf{B})$. For a static magnetic field applied along the z direction, we shall see that the local spin would precess about the field in the absence of friction. The coupling matrix then becomes:

$$\hat{\Omega} = \begin{pmatrix} \Omega_{\uparrow\uparrow} & \Omega_{\uparrow\downarrow} \\ \Omega_{\downarrow\uparrow} & \Omega_{\downarrow\downarrow} \end{pmatrix} = \begin{pmatrix} \cos\theta & \sin\theta e^{-i\phi} \\ \sin\theta e^{i\phi} & \cos\theta \end{pmatrix} \,. \tag{2}$$

In Eq. (2), θ is the angle between μ and $\mathbf{B}$, and $\phi = -\omega_L t + \phi_0$ with $\omega_L = \gamma B$ the Larmor frequency and ϕ_0 an initial azimuthal angle. If friction is present between the spin and its environment, the local spin would eventually become parallel to the field. The friction corresponds to the relaxation processes characterized by time T. We assume that T is sufficiently long for the precession to be well defined. As the energy associated with the spin precession, $\hbar\omega_L \sim 10^{-6}$ eV, is much smaller than the typical electronic energy on the order of 1 eV, the spin precession is very slow as compared to the time scale of all conduction electron process. This allows us to treat the electronic problem adiabatically as if the local spin is static for every instantaneous spin orientation.[10] Our aim is to calculate the conductance through the spin impurity. In a generalized Büttiker-Landauer formalism,[11,12] it can be expressed as[13]:

$$g = \frac{e^2}{h} \int d\epsilon f'_{\text{FD}}(\epsilon) \text{Im}[\text{Tr}\{\frac{2\hat{\Gamma}_L \hat{\Gamma}_R}{\hat{\Gamma}_L + \hat{\Gamma}_R} \hat{G}^r(\epsilon)\}] \,. \tag{3}$$

Equation (3) expresses the linear-response conductance in terms of the transmission probability weighted by the derivative of the Fermi distribution function, $f_{\text{FD}} = 1/\{\exp[(\epsilon - \mu)/k_B T] + 1\}$, with μ the chemical potential in the equilibrium state. The transmission probability is constructed as a product of the elastic coupling to the

leads and the Green function of electrons on the spin impurity site. The coupling to the leads is represented by the full line-width function:

$$\Gamma^{L(R)}_{\sigma\sigma'} = 2\pi \sum_{k,\sigma'' \in L(R)} V^*_{k,\sigma'';\sigma} V_{k,\sigma'';\sigma'} \delta(\epsilon - \epsilon_k) \; . \tag{4}$$

Here we assumed that the couplings to the left and right leads are factorizable, i.e., $\hat{\Gamma^L} = \lambda \hat{\Gamma^R}$.[13] The quantity in Eq. (3) $\hat{G}^r(\epsilon)$ is the Fourier transform of the retarded Green function for electrons on the spin impurity site:

$$G_{\sigma\sigma'} = -i\Theta(t)\langle [d_\sigma(t), d^\dagger_{\sigma'}(0)]_+ \rangle \; , \tag{5}$$

where $[\ldots]_+$ is the anticommutator, $\Theta(t)$the Heaviside step function, and $d^\dagger_\sigma(t)$ $(d_\sigma(t))$ the impurity-site electron operators in the Heisenberg picture, e.g., $d_\sigma(t) = e^{iHt} d_\sigma e^{-iHt}$. Both $\hat{\Gamma}$ and $\hat{G}^r$ are matrices in the spin space of the impurity-site electron. The remaining task is to evaluate the impurity-site electron Green function. This calculation should be done in the presence of the coupling to leads. We employ the equations-of-motion method to this end. We differentiate $G_{\sigma\sigma'}$ with respect to time, thereby generating new Green functions. As we show below, in the absence of electron correlation, the equations of motion for $G_{\sigma\sigma'}$ can be closed exactly. Otherwise, the higher-order equations-of-motion arising from electron correlation must be truncated to close the equations-of-motion for $G_{\sigma\sigma'}$. Using the commutator $[d_\sigma, H]_-$, we find the equation of motion for $G_{\sigma\sigma'}$:

$$i\frac{\partial G_{\sigma\sigma'}(t)}{\partial t} = \delta(t)\delta_{\sigma\sigma'} + J\sum_{\sigma''} \Omega_{\sigma\sigma''} G_{\sigma''\sigma'}(t) + \sum_{k,\sigma'' \in L(R)} V^*_{k,\sigma'';\sigma} G_{k\sigma'',\sigma'}(t) \; . \tag{6}$$

The derivative of $G_{\sigma\sigma'}$ generates a Green function describing the coupling of the impurity site to the leads,

$$G_{k\sigma,\sigma'} = -i\Theta(t)\langle [c_{k\sigma}(t), d^\dagger_{\sigma'}(0)]_+ \rangle \; . \tag{7}$$

Using the commutator $[c_{k\sigma}, H]_-$,

$$i\frac{\partial G_{k\sigma,\sigma'}(t)}{\partial t} = \epsilon_k G_{k\sigma,\sigma'}(t) + \sum_{\sigma''} V_{k\sigma,\sigma''} G_{\sigma''\sigma'}(t) \; . \tag{8}$$

Eq. (6) for $G_{k\sigma,\sigma'}$ now closes with the aid of Eq. (8). Fourier transforming these equations, we obtain

$$\omega G_{\sigma\sigma'}(\omega) = \delta_{\sigma\sigma'} + J\sum_{\sigma''} \Omega_{\sigma\sigma''} G_{\sigma''\sigma'}(\omega) + \sum_{k,\sigma'' \in L(R)} V^*_{k,\sigma'';\sigma} G_{k\sigma'',\sigma'}(\omega) \; , \tag{9}$$

$$\omega G_{k\sigma,\sigma'}(\omega) = \epsilon_k G_{k\sigma,\sigma'}(\omega) + \sum_{\sigma''} V_{k\sigma,\sigma''} G_{\sigma''\sigma'}(\omega) \; . \tag{10}$$

A little algebra yields the solution:

$$G_{++}(\omega) = \frac{1}{\omega - (J\Omega_{++} + \Sigma_{++}) - \Sigma_1}, \quad G_{+-}(\omega) = \frac{(J\Omega_{+-} + \Sigma_{+-})G_{--}(\omega)}{\omega - (J\Omega_{++} + \Sigma_{++})} \; , \tag{11}$$

$$G_{-+}(\omega) = \frac{(J\Omega_{-+} + \Sigma_{-+})G_{++}(\omega)}{\omega - (J\Omega_{--} + \Sigma_{--})}, \quad G_{--}(\omega) = \frac{1}{\omega - (J\Omega_{--} + \Sigma_{--}) - \Sigma_2} \; . \tag{12}$$

In Eq. (12), the self-energy matrix due to the coupling to the leads is:

$$\Sigma_{\sigma\sigma'}(\omega) = \sum_{k,\sigma'' \in L,R} \frac{V^*_{k\sigma'',\sigma} V_{k\sigma'',\sigma'}}{\omega - \epsilon_k} \; , \tag{13}$$

$$\Sigma_1(\omega) = \frac{(J\Omega_{+-} + \Sigma_{+-})(J\Omega_{-+} + \Sigma_{-+})}{\omega - (J\Omega_{--} + \Sigma_{--})}, \quad \Sigma_2(\omega) = \frac{(J\Omega_{-+} + \Sigma_{-+})(J\Omega_{+-} + \Sigma_{+-})}{\omega - (J\Omega_{++} + \Sigma_{++})} \; . \tag{14}$$

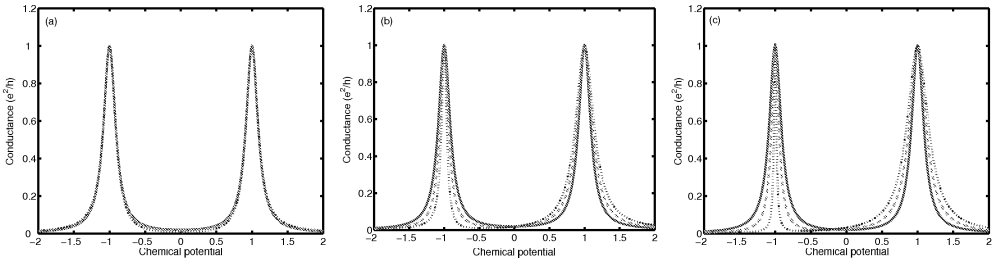

Figure 2. Conductance versus the chemical potential μ with various values of the spin-flip coupling $\Gamma_s/\Gamma_n = 0.0$ (red-solid line), 0.4 (green-dashed line), and 0.8 (blue-dotted line). The results shown in panels (a) through (c) correspond to three different local spin orientations in zero magnetic field: (θ, ϕ_0)=(0,0), $(\pi/4, 0)$, $(\pi/2, 0)$. The spin-conserved coupling, $\Gamma_n = 0.1$.

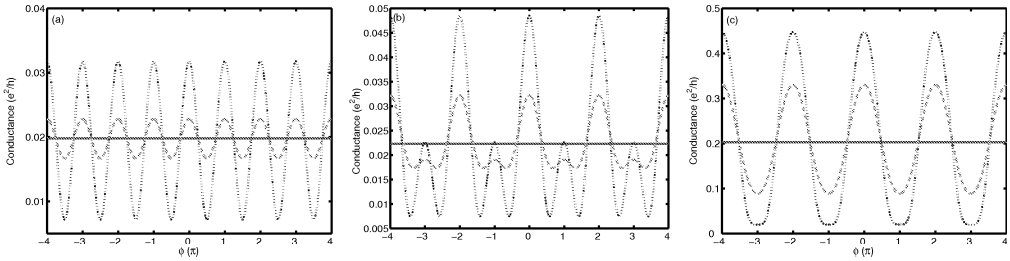

Figure 3. Conductance (in units of e^2/h) versus the phase ϕ (in multiples of π) accumulated by the precession of the local spin with various values of the spin-flip coupling $\Gamma_s/\Gamma_n = 0.0$ (red-solid line), 0.4 (green-dashed line), and 0.8 (blue-dotted line). The results shown in the left panels (a) through (c) correspond to three different values of the chemical potential: $\mu = 0$, 0.4, and 0.8. Also shown in the right panels is the Fourier spectrum for $\Gamma_s/\Gamma_n = 0.4$ with the chemical potential same as in the left panels. Other parameter values: $\Gamma_n = 0.1$, $\theta = \pi/2$, and $\phi_0 = 0$.

Equation (13) shows that the structure of the self energy is determined by the nature of the tunneling matrix elements $V_{k\sigma,\sigma'}$. The retarded self energy can be written in terms of the principle and imaginary parts:

$$\Sigma^r_{\sigma\sigma'}(\omega) = \mathcal{P} \sum_{k,\sigma'' \in L,R} \frac{V^*_{k\sigma'',\sigma} V_{k\sigma'',\sigma'}}{\omega - \epsilon_k} - \frac{i}{2}[\Gamma^L_{\sigma\sigma'}(\omega) + \Gamma^R_{\sigma\sigma'}(\omega)] \,, \tag{15}$$

where the full line-width functions have been given by Eq. (4). The solution for $\hat{G}^r(\omega)$, as given by Eq. (12), can now be employed to evaluate the conductance by Eq. (3). The structure of the full line-width functions , $\hat{\Gamma}^{L,R}$, is determined by the details of the tunneling matrix $V_{k\sigma,\sigma'}$. We use the full line-width functions as the coupling parameters. The full retarded self-energies $\hat{\Sigma}^r$ are evaluated according to Eq. (15). For simplicity, we assume symmetric tunneling barriers between the local spin and the leads, therefore, $\hat{\Gamma}^L = \hat{\Gamma}^R = \hat{\Gamma}$. As the density of states around the Fermi surface in the leads is broad and flat, the couplings are constant. In the following, we measure the energy in units of the exchange integral between the electrons and the local spin, J, and consider the conductance at zero temperature. In zero magnetic field, the spin is static. In Fig. 2, we plot the conductance versus the chemical potential with various values of the spin-flip coupling $\Gamma_{+-} = \Gamma_{-+} = \Gamma_s$. The results in panels (a)-(c) correspond to the three different spin orientations: (θ, ϕ_0)=(0,0), $(\pi/4, 0)$, $(\pi/2, 0)$. The spin-conserved couplings are taken to be $\Gamma_{++} = \Gamma_{--} = \Gamma_n = 0.1$. From Fig. 2, a generic feature of the conductance is evident: As μ passes through ± 1, the conductance exhibits the resonant behavior by showing a peak at these energy position. The resonant level position is independent of the local-spin orientation. The spin-flip couplings does not change the resonant level position either. However, they change the line-width of the resonant peaks. Explicitly, with the increasing spin-flip couplings, the resonant peak at -1 is narrowing while that at $+1$ is broadening, but both with the maximum peak intensity almost unchanged.

As we showed, in the presence of magnetic field, the local spin will precess with the Larmor frequency. The

question is whether this Larmor precession will manifest in the conductance of electrons transported through this local spin, which we now address below. To be relevant to the experimental situation, we consider the electron tunneling in the off-resonance regime by choosing the value of the chemical potential other than ± 1. In Fig. 3, we plot the conductance as a function of the phase ϕ accumulated by the precession of the local spin for various values of the spin-flip couplings. Without loss of generality, we have taken $\theta = \pi/2$ and $\phi_0 = 0$. The results shown in the left panels (a)-(c) correspond to three typical values of the chemical potential μ=0, 0.4, and 0.8. Also shown in the right panels is the Fourier spectrum for a fixed value $\Gamma_s/\Gamma_n = 0.4$ with the chemical potential same as in the left panels. Several features are noteworthy: (i) The conductance oscillation occurs only when the spin-flip couplings is nonzero and its oscillation amplitude increases with the spin-flip couplings. (ii) When $\mu = 0$, the conductance exhibits the periodicity of π (see Fig. 3(a)), which corresponds to the oscillation of frequency $2\omega_L$. When μ is nonzero, the conductance oscillates in phase with a basis period of 2π, that is, with frequency ω_L (see Fig. 3(b) and (c)). Generally, there still exists of the $2\omega_L$ mode, the Fourier spectral weight of which decreases with the deviation of μ from zero but is enhanced by the spin-flip couplings. These modes can be seen more clearly from the Fourier spectrum. Analytically, we find that the imaginary part of the off-diagonal components of the retarded Green function satisfy $\mathrm{Im}G^r_{+-}(\phi+\pi) = \mathrm{Im}G^r_{-+}(\phi)$. Therefore, $\mathrm{Im}[G^r_{+-} + G^r_{-+}]$ is a periodic function of ϕ with a period of π. However, the periodicity of $\mathrm{Im}G^r_{++}$ and $\mathrm{Im}G^r_{--}$ depends on the position of the chemical potential. With a little algebra, one can obtain:

$$\mathrm{Im}[G^r_{++} + G^r_{--}] = \frac{-4\omega(J\sin\theta\Gamma_s\cos\phi + \omega\Gamma_n) + 2\Gamma_n\tilde{\omega}^2}{\tilde{\omega}^4 + 4(J\sin\theta\Gamma_s\cos\phi + \omega\Gamma_n)^2}\ , \tag{16}$$

and $\tilde{\omega} = [\omega^2 - J^2 - \Gamma_n^2 + \Gamma_s^2]^{1/2}$. Equation (16) shows that the contribution to the conductance from the spin-conserved couplings involves the linear term and quadratic term in $\cos\phi$. When $\omega = 0$, the linear term vanishes, and the oscillation is determined solely by the $\cos^2\phi$ term. This explains why the conductance oscillates with frequency $2\omega_L$ as $\mu = 0$. Moreover, since the contributions to the conductance from $\mathrm{Im}[G^r_{++} + G^r_{--}]$ and $\mathrm{Im}[G^r_{+-} + G^r_{-+}]$ are weighted by Γ_n and Γ_s, respectively, one can expect that the spectral weight of $2\omega_L$ mode in the conductance oscillation is appreciable for a large ratio of Γ_s/Γ_n even when $\mu \neq 0$.

To conclude, we studied the quantum transport through a local impurity spin precessing in an external static magnetic field. We found that the spin-flip coupling between the conduction electrons on the spin and those in the leads are crucial to the appearance of the conductance oscillation. We predict the existence of an oscillation mode with a frequency *twice of the Larmor frequency*, the Fourier spectral weight of which can be tuned by the position of the chemical potential and spin flip coupling. In reality, the dynamics of the local spin is also influenced by the backaction of the transport currents due to its coupling to the conduction electrons. Our results should be valid in the weak measurement regime, where the spin relaxation time is sufficiently long. In the opposite regime, the interactions of the spin with its surroundings are so strong that the spin precession will die out quickly and the spin is aligned with the magnetic field **B**. We can then apply a small r.f. field perpendicular to the static magnetic field. By solving the Bloch equation, one can find the transverse components of the spin oscillate with the r.f. frequency. This leads to an exchange interaction between a driven spin and conduction electrons very similar to that given by Eq. (2). The conductance can be evaluated by following the same procedure and the conclusion about the conductance oscillation remains. This setup is experimentally accessible, and its measurement will provide an additional test of the proposed mechanism for the conductance oscillation.

3. SPIN NUTATIONS IN A JOSEPHSON JUNCTION

In this section, we predict the nutation of single spin by a Josephson current (*Josephson nutations*). Potentially, this might be important for the interception of the information stored on the spin. As in the previous section, the model system under consideration is illustrated in Fig. 1. Now, however, it consists of two ideal *superconducting* leads coupled to each other by a single magnetic spin. In the presence of a magnetic field, the spin precesses around the field direction. We neglect the interaction of the spin with two superconducting leads. The Hamiltonian for the Josephson junction can be written as[14, 15]: $H = H_L + H_R + H_T$. The first two terms are the Hamiltonians for electrons in the left and right superconducting leads $H_{L(R)} = \sum_{k(p);\sigma}\epsilon_{k(p)}c^\dagger_{k(p),\sigma}c_{k(p),\sigma} + \frac{1}{2}\sum_{k(p);\sigma,\sigma'}[\Delta_{\sigma\sigma'}(k(p))c^\dagger_{k(p),\sigma}c^\dagger_{-k(-p),\sigma'} + \mathrm{H.c.}]$, where, similar to the previous section, we denote the electron creation (annihilation) operators in the left (L) lead by $c^\dagger_{k\sigma}$ ($c_{k\sigma}$) while those in the

right (R) lead by $c^\dagger_{p\sigma}$ ($c_{p\sigma}$). The quantities k (p) are momenta, σ the spin index, and $\epsilon_{k(p),\sigma}$, $\Delta_{\sigma\sigma'}(k(p))$ are, respectively, the single particle energies of conduction electrons, and the pair potential in the leads. In this work, we consider s-wave pairing symmetry in the superconducting leads. The two leads are weakly coupled via the tunneling Hamiltonian: $H_T = \sum_{k,p;\sigma,\sigma'}[T_{\sigma\sigma'}(k,p)c^\dagger_{k\sigma}c_{p\sigma'} + \text{H.c.}]$, where the matrix element $T_{\sigma\sigma'}(k,p)$ transfer electrons through an insulating barrier. When a spin is embedded in the tunneling barrier, the tunneling matrix becomes a spin operator[10]: $\hat{T} = T_0\delta_{\sigma\sigma'} + T_1\mathbf{S}\cdot\sigma_{\sigma\sigma'}$, where T_0 is a spin-independent tunneling matrix element and T_1 is a spin-dependent matrix element originating from the direct exchange coupling J of the conduction electron to the localized spin $\mathbf{S}$. We take both to be momentum independent. This is not a crucial assumption and is merely introduced to simplify notations. Typically, from the expansion of the work function for tunneling, $\frac{T_1}{T_0} \sim J/U$, where U is a spin-independent tunneling barrier.[16] We further allow a weak external magnetic field $B \sim 10^2$ Gauss. Such a small field will not influence the superconducting state and we may ignore its effect on the leads. The Josephson junction with the spin has two time scales: (i) The Larmor precession frequency of the spin $\omega_L = g\mu_B B$, where g, μ_B are the gyromagnetic ratio and Bohr magneton of the conduction electron, respectively. (ii) The frequency $\omega_J = 2eV$ characterizing the Josephson effect when an external voltage V applied.

We now derive the effective action via the Keldysh technique. If all external fields are the same on both forward and backward branches of the Keldysh contour (C) then $\mathcal{Z} = \text{Tr}\, T_C \exp[-i\oint_C dt H_T(t)] = 1$, where the trace is over both the electron and the spin degrees of freedom. We first take a partial trace in $\mathcal{Z}$ over the lead fermions (the bath) to obtain an effective spin action. The Josephson contribution to the resulting spin action reads $i\delta\mathcal{S} = -\frac{1}{2}\oint_C dt \oint_C dt' \langle T_C H_T(\mathbf{S}(t),t)H_T(\mathbf{S}(t'),t')\rangle$, much in the spirit of Refs..[17,18] For brevity, we set $A_{\sigma,\sigma'} \equiv \sum_{k,p} c^\dagger_{k\sigma}c_{p\sigma'}$. The tunneling Hamiltonian of a phase (voltage) biased junction

$$H_T \;=\; [T_0\delta_{\sigma\sigma'} + T_1\mathbf{S}\cdot\sigma_{\sigma\sigma'}]\big(\mathbf{A}_{\sigma\sigma'}\exp(\mathbf{i}\phi/\mathbf{2}) + \mathbf{A}^\dagger_{\sigma\sigma'}\exp(-\mathbf{i}\phi/\mathbf{2})\big)\,. \tag{17}$$

In the presence of a dc voltage bias, $\phi = 2eVt$. As ϕ is treated classically (i.e. ϕ is the same on the upper and the lower branches of the Keldysh contour), the contribution $\propto T_0^2$ to $\delta\mathcal{S}$ vanishes. The mixed contribution $\propto T_0T_1$ vanishes due to the singlet spin structure of the s-wave superconductor. The only surviving contribution reads

$$i\delta\mathcal{S} = -\tfrac{T_1^2}{2}\oint_C dt\oint_C dt'\,[\mathbf{S}(t)\cdot\sigma_{\alpha\beta}]\,[\mathbf{S}(t')\cdot\sigma_{\delta\gamma}]\left(\langle T_C A_{\alpha\beta}(t)A_{\delta\gamma}(t')\rangle e^{i\frac{\phi(t)+\phi(t')}{2}} + (A,\phi\to A^\dagger,-\phi)\right) \tag{18}$$

where we keep only the Josephson (off-diagonal) terms. The spin structure simplifies for the s-wave case:

$$i\delta\mathcal{S} = T_1^2\oint_C dt\oint_C dt'\,[\mathbf{S}(t)\cdot\mathbf{S}(t')]\,[iD(t,t')]\,, \tag{19}$$

where $iD(t,t') \equiv \langle T_C A_{\uparrow\uparrow}(t)A_{\downarrow\downarrow}(t')\rangle e^{i\frac{\phi(t)+\phi(t')}{2}} + (A,\phi\to A^\dagger,-\phi)$. Next, we perform the standard Keldysh manipulations, defining upper and lower spin fields $\mathbf{S}^{u,l}$ residing on the forward/backward contours and reducing the time ordered integral over Keldysh contour to the integral over forward running time at the cost of making the Green's function G a 2×2 matrix. Finally, after a rotation to the classical and quantum components

$$\mathbf{S}_1 \equiv (\mathbf{S}^u + \mathbf{S}^l)/2,\;\; \mathbf{S}_2 \equiv \mathbf{S}^u - \mathbf{S}^l,\;\; \mathbf{S}_1\cdot\mathbf{S}_2 = 0, \tag{20}$$

we obtain $i\delta\mathcal{S} = i\mathcal{S}_R + \mathcal{S}_I$, where

$$i\mathcal{S}_R = \int\int dtdt'\,\mathbf{S}_2(t)\cdot\mathbf{S}_1(t')[iK_{12}(t,t')]. \tag{21}$$

with $K_{12}(t,t') = T_1^2\,[D^R(t,t') + D^A(t',t)]$, and

$$\mathcal{S}_I = \frac{1}{2}\int\int dtdt'\mathbf{S}_2(t)\cdot\mathbf{S}_2(t')[iK_{22}(t,t')], \tag{22}$$

with $K_{22}(t,t') = T_1^2\,D^K(t,t')$. The retarded (R) and Keldysh (K) components are defined via

$$\begin{aligned} iD^R(t,t') &= \Theta(t-t')\langle[A_{\uparrow\uparrow}(t),A_{\downarrow\downarrow}(t')]_-\rangle e^{i\frac{\phi(t)+\phi(t')}{2}} - \text{c.c.}\,,\\ iD^K(t,t') &= \langle\{A(t)_{\uparrow\uparrow},A_{\downarrow\downarrow}(t')\}_+\rangle e^{i\frac{\phi(t)+\phi(t')}{2}} + \text{c.c.} \end{aligned} \tag{23}$$

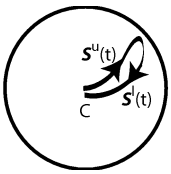

Figure 4. The unit sphere for the vectors $\mathbf{n}^{u,l}(t)$ is shown. The contour C is the Keldysh contour for the forward (u) and backward (l) evolution. To properly describe the spin on this closed contour we analyze the WZWN term, see Eq. (27). For clarity, we draw a small piece of the closed trajectories.

The advanced component in our case is simply $iD^A(t,t') = iD^R(t',t)$. The kernels K_{12} and K_{22} are readily calculated at $T=0$ from $\mathcal{A} \equiv \langle A(t)_{\uparrow\uparrow} A_{\downarrow\downarrow}(t')\rangle = \sum_{k,p} \frac{|\Delta|^2}{4E_k E_p} e^{-i(E_k+E_p)(t-t')}$, where $E_{k(p)} = \sqrt{(\epsilon_{k(p)} - E_F)^2 + |\Delta|^2}$. As only frequencies higher than 2Δ are present in $\mathcal{A}$, the imaginary component S_I (Eq. (22)) vanishes for slow fluctuations of $\mathbf{S}_2$- unlike the real part of the action S_R (due to the presence of Θ function in Eq. (23)).

To properly describe the dynamics of the spin fields $\mathbf{S}_1$ and $\mathbf{S}_2$, we employ the path integral representation for the spin fields.[19,20] The action for a free spin consists of two terms $\mathcal{S}_0 = g\mu_B \oint_C dt \mathbf{B}\cdot\mathbf{S} + \mathcal{S}_{WZWN}$. The second, Wess-Zumino-Witten-Novikov (WZWN), term describes the Berry phase accumulated by the spin as a result of motion of the spin on the sphere.[19,20] We generalize this action for nonequlibrium dynamics within the Keldysh contour formalism (Fig. 4). We write the WZWN term on both forward and backward contours, and consequently analyze matters in terms of $\mathbf{S}_1$ and $\mathbf{S}_2$,

$$i\mathcal{S}_{WZWN} = \frac{i}{S^2}\int_0^1 d\tau \int dt[\mathbf{S}^u(t,\tau)\cdot(\partial_\tau \mathbf{S}^u(t,\tau)\partial_t \mathbf{S}^u(t,\tau)) - (u\to l)]\,. \tag{24}$$

The relative minus sign stems from the backward time ordering on the return part of C. The spins $\mathbf{S}^{u,l} = S\mathbf{n}^{u,l}$ with S the magnitude of the spin and $\mathbf{n}^{u,l}$ a unit vector field. The additional integral over τ permits us to express the action in a local form. At $\tau = 0$ we set the spin to point along the z direction at all times; at $\tau = 1$ the spin field corresponds to the physical configurations. Each of the individual WZWN phases (for both the forward (u) and backward (l) branches) is the spin magnitude (S) multiplied by the areas spanned by the trajectories $\mathbf{n}^{u,l}(t)$ on the unit sphere. The WZWN term contains *odd* powers of $\mathbf{S}_2$. Insofar as the WZWN term of Eq.(24) is concerned, the standard Keldysh transformation to the two classical and quantum fields, $\mathbf{S}_1$ and $\mathbf{S}_2$, mirrors the decomposition of the spin in an antiferromagnet (AF) to the two orthogonal slow and fast fields. The difference between the two individual WZWN terms in Eq.(24) is the area spanned between the forward and backward time trajectories. The magnitude of this area traced between times t and $t+\delta t$ is

$$\delta\mathcal{S}_{WZWN} = S(\delta t)\delta\mathbf{n}\cdot(\mathbf{n}\times\partial_t\mathbf{n}). \tag{25}$$

Here, the variation between the forward and backward trajectory at a given instant of time is $\delta\mathbf{n} = \mathbf{S}_2/S$. In Eq.(25), we note that for small variations between the forward and backward trajectories, $\mathbf{n} = \mathbf{S}_1/S$. The WZWN action on the Keldysh loop may be expressed as

$$\mathcal{S}_{WZWN} = \frac{1}{S^2}\int dt\,\mathbf{S}_2\cdot(\mathbf{S}_1\times\partial_t\mathbf{S}_1). \tag{26}$$

The real part of the total action, $\mathcal{S}_{cl} \equiv \mathcal{S}_0 + \mathcal{S}_R$, determines the quasi-classical equation of motion. The imaginary part of the action $\mathcal{S}_I$ is usually responsible for the Langevin stochastic term. In our case, however, the Langevin term is suppressed at frequencies much lower than Δ. The fluctuations of $\mathbf{S}_2$ are not suppressed by the bath and no dissipation appears. The only reason to consider small fluctuations of $\mathbf{S}_2$ is the dominance of the quasi-classical trajectories determined by $\mathcal{S}_{cl}$. Thus our analysis applies for large spins. The classical action

$$\mathcal{S}_{cl} = \mathcal{S}_{WZWN} + g\mu_B\int dt\mathbf{B}\cdot\mathbf{S}_2 + \int dt\int dt' K_{12}(t,t')\mathbf{S}_2(t)\cdot\mathbf{S}_1(t'). \tag{27}$$

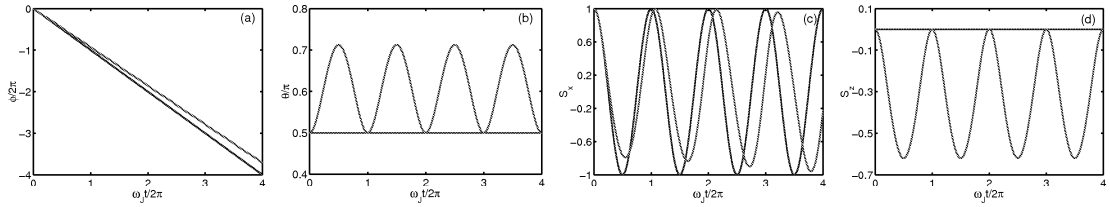

Figure 5. The spin dynamics. Top panels: the azimuthal (ϕ) and polar (θ) angles as a function of time for an exaggerated $\alpha = 0.4$ (red) versus the standard precessions in the absence of the coupling ($\alpha = 0$ in blue). Note that unlike the standard case, the semi-classical spin trajectory is not confined to planar motions. The polar angle oscillates between its two extreme values θ_1 and θ_2. In the bottom panels we display $\langle S_x(t)\rangle$ and $\langle S_z(t)\rangle$. Here we take $\omega_L = \omega_J$.

As in the previous section, the spin dynamics is much slower as compared to electronic processes. We thus set $\mathbf{S}_1(t') \simeq \mathbf{S}_1(t) + (t'-t)d\mathbf{S}_1/dt$. The variational equations $\delta S_{cl}/\delta \mathbf{S_2}(t) = 0$ imply

$$\frac{d\mathbf{n}}{dt} = \alpha \mathbf{n} \times \frac{d\mathbf{n}}{dt} \sin\omega_J t + g\mu_B \mathbf{n} \times \mathbf{B}, \tag{28}$$

where henceforth we denote $\mathbf{S}_1$ by $\mathbf{S} = S\mathbf{n}$, and $\alpha = S\sum_{k,p} \frac{|\Delta|^2 |T_1|^2}{E_k E_p}[(E_k + E_p - eV)^{-2} - (E_k + E_p + eV)^{-2}]$. The non-dissipative term proportional to α in Eq. (28) arises from superconducting retardations. Both $\mathbf{S} \times \frac{d\mathbf{S}}{dt}$ and $I \sim \sin\omega_J t$ are odd in time and their product is allowed in the equation of motion. Due to the spectral gap, dissipation is faint at low temperatures and frequencies. The classical equation of motion, Eq. (28), implies that $\mathbf{n} \cdot d\mathbf{n}/dt = 0$, as it must to be consistent with the parameterization of the spin on the sphere, $S\mathbf{n} = S(\sin\theta\cos\phi, \sin\theta\sin\phi, \cos\theta)$. Orienting the z-axis along the external magnetic field $\mathbf{B}$, Eq. (28) reads

$$\frac{d\phi}{dt} = -\frac{\omega_L}{1 + \alpha^2 \sin^2(\omega_J t)}, \quad \frac{d\theta}{dt} = -\alpha \frac{d\phi}{dt} \sin\theta \sin\omega_J t\,. \tag{29}$$

For a spin initially oriented at an angle θ_0 relative to $\mathbf{B}$,

$$\begin{aligned} \phi(t) &= -\frac{\omega_L}{\omega_J\sqrt{1+\alpha^2}} \tan^{-1}[\sqrt{1+\alpha^2}\tan(\omega_J t)], \\ \theta(t) &= 2\tan^{-1}\left(\left[\frac{(1 - c\cos(\omega_J t))(1+c)}{(1 + c\cos(\omega_J t))(1-c)}\right]^{\gamma} \tan\frac{\theta_0}{2}\right), \end{aligned}$$

with $c = |\alpha|/\sqrt{1+\alpha^2}$ and $\gamma = -\alpha\omega_L/2\omega_J c$. For $\alpha \ll 1$, $\phi \simeq -\omega_L t$ and $\theta \simeq \theta_0 - \alpha(\omega_L/\omega_J)\sin\theta_0 \cos\omega_J t$. Canonically, whenever a single spin is subjected to a uniform magnetic field, the spin azimuthally precesses with a frequency ω_L. In a Josephson junction, however, the spin exhibits additional polar (θ) displacements. The resulting dynamics (*Josephson nutations*) may be likened to that of a rotating rigid top. The Josephson current leads to a full non-planar gyroscopic motion (nutations) of the spin much like that generated by applied "torques" on a mechanical top. In Fig. 5, we display the resulting dynamics for the spin. A schematic of the generic spin motion is displayed in Fig. 6. Similar to a classical spinning top, the spin wobbles along the polar direction in addition to azimuthal rotations. Similar dynamics is even expected for a quantum $S = 1/2$. In a spin coherent state path integral, the Schrodinger equation is essentially classical.

We may directly monitor the spin dynamics by SQUID measurements. The spin motion generates a time dependent magnetic field, $\delta\mathbf{B}(\mathbf{r}, t) = \frac{\mu_0}{4\pi}[3\mathbf{r}(\mathbf{r}\cdot\mathbf{m}(t)) - r^2\mathbf{m}(t)]/r^5$, superimposed against the constant external field $\mathbf{B}$. Here, $\mathbf{r}$ is the position from the spin and the magnetic moment $\mathbf{m}(t) = g\mu_B S\mathbf{n}(t)$. For a ferromagnetic cluster of spin $S = 100$, a detectable field $\delta B \sim 10^{-10}$ Tesla appears in a SQUID placed a micron away. For a SQUID loop of micron dimensions, the corresponding flux variation $\delta\Phi \sim 10^{-7}\Phi_0$ (with Φ_0 a flux quantum) —within reach of modern SQUIDs. For such a setup with $(T_1/T_0) \sim 10^{-1}$, typical critical Josephson current $J_S^{(0)} \sim 10$ μA, $|\Delta| = 1.0$ meV, and $eV \sim 10^{-3}|\Delta|$, we find that $\alpha \sim 0.1$. As $n_x = \sin\theta\cos\phi$, with a similar relation for n_y, the spin components orthogonal to $\mathbf{B}$ vary, to first order in α, with a Fourier component at

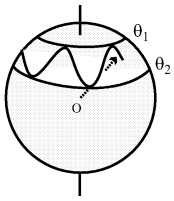

Figure 6. The resulting spin motion on the unit sphere in the general case. As in the motion of classical spinning top, the spin exhibits undulations along the polar direction.

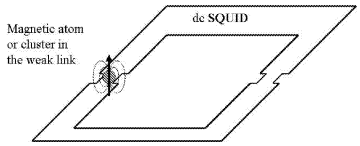

Figure 7. A SQUID-based detection scheme. The SQUID monitors the magnetic field produced by the magnetic cluster in one of the junctions.

frequency $|\omega_L \pm \omega_J|$, leading to a discernable signal in the magnetic field $(\mathbf{B} + \delta\mathbf{B})$. For a field $B \sim 200$ Gauss, $\omega_L \sim 560$ MHz wherein for a substantial voltage (ω_J) range, a new side band will appear at $|\omega_L - \omega_J|$ whose magnitude may be tuned to $\mathcal{O}(10 - 100)$ MHz. This measurable frequency is markedly different from that associated with standard Larmor frequency (ω_L) precessions. The efficiency of the detector may be improved by embedding the spin in one of the Josephson junctions of the SQUID. The setup is sketched in Fig. 7. The Josephson junction containing the spin is used both for driving the nutations and, together with the second junction of the SQUID, for detecting them.

To conclude, by analyzing WZWN phases within the non-equilibrium Keldysh framework, we find novel non-planar spin dynamics in the presence of a tunneling Josephson current (*Josephson nutations*). The coupling of the spin to a superconducting bath produces non-damping spin retardation. This retardation results from additional non-dissipative terms in the spin equations of motion. There are important differences with the case of Josephson effect in the presence of a vibrational mode.[21] The dynamics may be monitored by SQUID measurements.

4. SINGLE SPIN NOISE SPECTROSCOPY

In this section we propose to use a spin polarized STM tunnel current to gain spectroscopic information on a single magnetic atom on a non-magnetic surface. The set up is similar to the one used in recent ESR-STM experiments, although we now consider the same for spin polarized current. A scheme is depicted in Fig.(8). We start with a magnetic atom of spin **S** placed on an otherwise non-magnetic substrate. This system forms the analogue of Fig.(1) wherein the left lead is replaced by an STM tip and the right lead by the sybstrate. As we will explain, the noise in the current flowing from the STM tip will allow us, in certain instances, to directly measure the single spin time dependent susceptibility. This is yet another case where the spectroscopy of current noise allows us (where other methods often fail) to directly probe the highly disordered quantum states of a microscopic system (in this case a single spin). In earlier sections, we examined related systems in the presence of a small external magnetic field. Here we consider the situation at *a vanishing external field*, and within the context of a spin polarized tunnel current. Our work also differs in the former context from,[22] and further offers a transparant and accesible account of the underlying physics. Throughout this section we propose and analyze aspects of a new experimental technique for probing single spin dynamics. The outline of this section is as follows:

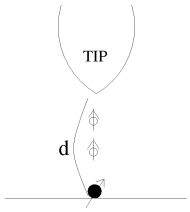

Figure 8. The experimental setup. The surface tip separation distance is d. The single magnetic atom on the surface is marked by a solid circle. The spin polarized current emanating from the STM tip is shown by the spin up open symbols.

In subsection(4.1), we derive the general relation between the noise $\langle|\delta I(\omega)|^2\rangle$ in the current and the single spin susceptibility $\chi(\omega)$. Under quite general circumstances, the noise in the current is directly proportional to the single spin susceptibility, so that measuring the noise in the current immediately gives us valuable information about the single spin susceptibility. In subsection 4.2, we will elaborate on the origin of the spin dependent tunneling matrix elements that form much of the backbone of our proposal. In subsection 4.3, we will discuss the decoherence resulting from backaction effects. Here, we will also relate the spin scattering relaxation rate and DC charge transport and estimate how large the various quantities might be in realistic setups. We will conclude, in subsection 4.4, by evaluating the typical signal to noise ratios for our experimental proposal.

4.1. How to probe the Spin Susceptibility via a measurement of the noise

There is a major difference between probing a single spin (as discussed here) and probing a macroscopic magnetic system. In the case of a single atomic spin $\mathbf{S}(t)$, we perform a measurement on a microscopic state that is quantum and highly fluctuating due to interactions with its environment. The tunneling experiment discussed here is a specific example of *noise spectroscopy*, wherein we extract spectroscopic information, such as the single spin relaxation time T^* from the measurement of the noise in the current. The main idea of noise spectroscopy in STM is that the time dependence of the tunneling current will have a characteristic relaxation time that is directly related to spin relaxation time T^*. Here T^* does not originate from a directly applied external magnetic field (there is none) but rather from substrate excitations and other effects. The time varying tunneling current $I(t)$ will have a fluctuating component, apart from its average DC value I_0. Current noise is given by the Fourier transform of the time-dependent fluctuations of the electrical current leading to the power spectra $\langle|\hat{I}(\omega)|^2\rangle$ within the frequency domain. Here, we will focus on the power spectrum of the tunneling current and argue that it is proportional to the local spin susceptibility, $\chi(\omega) = \langle \mathbf{S}_\omega \cdot \mathbf{S}_{-\omega}\rangle = \frac{1/T^*}{\omega^2+1/T^{*2}}$, of the single atom on the substrate. In the above, T^* denotes the relaxation time to the polarization axis of the single local spin (for a macroscopic collection of spins, this would be none other than the standard T_1 of NMR gauging the relaxation time to the polarization axis). We reiterate that in the present discussion there is a direct externally applied magnetic field T^*, and albeit the similarity the origin of the relaxation time here and in NMR of a completely different origin. A long time exponential relaxation for $\chi(t) \equiv \langle S(t)S(0)\rangle \sim \exp[-t/T^*]$, has as its Fourier transform the above Lorentzian form for $\chi(\omega)$. In this Lorentzian form, the inverse relaxation time $(T^*)^{-1}$ trivially appears as the linewidth of $\chi(\omega)$. If additional short time spin modulations occur, these will augment $\chi(\omega)$ by additional high frequency terms. In what follows, most of our focus will be on the long time (short frequency) behavior of the current noise. In thermal noise, the spectral density $\langle|I(\omega)|^2\rangle$ is independent of frequency (e.g. being $4k_BT/R$ at a temperature T for current flowing through a resistor of magnitude R). Shot noise, on the other hand, results from the discrete pulse-like character of electrical current. Its magnitude exhibits a white noise (frequency independent) spectrum that is proportional to the average DC current, $\langle|\hat{I}(\omega)|^2\rangle \simeq aeI_0$ (where the numerical constant $a = 2$ for a simple conductor), up to a certain cut-off frequency which is related to the time required for an electron to travel through the conductor. Examples of noise spectroscopy include the noise NQR measurements,[23] noise in Faraday rotation[24] and, recently, noise spectroscopy of a local spin dynamics in STM.[25] The central feature present in all of these examples is that the quantum system is not driven by external fields. Rather, the noise in the signal itself (e.g. thermal, shot, ...) sans any applied polarizing field allows us to extract spectroscopic information. Here we consider the excess noise produced by a single spin whose time-dependent quantum state we wish to probe. We suggest that over a certain parameter range, the excess noise generated

by the single spin will be the dominant noise source in a single spin tunnel junction. To make matters concrete, consider the tunneling between two contacts in the presence of a localized spin $\mathbf{S}$. The Hamiltonian, similar to those present in earlier sections, assumes the form

$$\hat{H} = \{\sum_{n\sigma} \epsilon_{Ln\sigma} c^{\dagger}_{Ln\sigma} c_{Ln\sigma} + \sum_{nn'\alpha\beta} c^{\dagger}_{Ln\alpha}[T_0 + T_1 \mathbf{S}\cdot\sigma_{\alpha\beta}]c_{Rn'\beta}\} + (L \to R). \tag{30}$$

In the above, $\sigma_{\alpha\beta}$ is the Pauli matrix vector with matrix indices α and β, the fermionic $c_{\lambda n\sigma}, c^{\dagger}_{\lambda n\sigma}$ are the annihilation and creation operators of electrons in the n-th eigenstate of the lead $\lambda = L, R$ with $\sigma = \pm 1$ the (up/down) spin polarization label. The left lead (L) is the STM tip, and the right lead (R) refers to the surface. For infinite "free" leads, the eigenstates $\{|n\rangle\}$ simply correspond to the various plane wave states $\{|\mathbf{k}\rangle\}$. In real systems, all hopping matrices $\hat{T}$ will carry additional n, n' labels. However, to make the notation more compact we will dispense with these indices. The wavefunctions of our system are superpositions of the direct product states $|\psi_L\rangle \otimes |\psi_S\rangle \otimes |\psi_R\rangle$ - the direct product of the state of the left contact, the impurity spin, and the right contact. The tunneling matrix $\hat{t}$ present in the second term of Eqn.(30) couples all of these different states. It has two contributions: the term proportional to T_0 describes the spin independent tunneling while the term proportional to T_1 depicts the spin dependent contributions arising from the exchange interaction for electrons tunneling to the magnetic atom. Only the second term in Eqn.(30) will give rise to net current flow from the left to the right contact. In section(4.2), we will explain the origin and elaborate on the magnitude of the spin independent and dependent terms. A chemical potential shift (voltage drop) between the two bands $\{\epsilon_{nL}\}$ and $\{\epsilon_{nR}\}$ will lead to a DC current within the steady state. Henceforth, we will assume that the tunneling electrons are partially spin polarized. There are several situations where such interactions may materialize. In a ferromagnetically coated tip a chemical potential difference $2(\delta\mu_\sigma)$ separates the two different spin polarizations: $\epsilon_{Ln\sigma} = \epsilon_{Ln} + \sigma\delta\mu_\sigma$. Ferromagnetically ordered tips have proven to be very successful in the study of magnetic structures.[2] Very recently, an alternative approach using antiferromagnetically coated tips with no ferromagnetic order has been used to produce spin polarized current.[26] These tips might have potential benefits as compared to ferromagnetic tips. A ferromagnetic tip may produce a field of $\mathcal{O}(1)$ Tesla at a separation of few angstroms from the surface. Ferromagnetic tips may therefore lead huge precession frequencies that are difficult to measure. In the case of an antiferromagnetic tip, there is a vanishing dipolar field. Both of these techniques may be used for the measurements proposed here. In what follows, we are not interested in a specific model for how the spin polarized current is generated. We define a parameter A that relates the spin polarized current to the net tunneling current. It is this parameter that will be determined by a particular microscopic model of the tip. Hereafter, we will treat A as a phenomenological parameter. As may be seen by examining the spin dependent contribution to $\hat{T}$, the tunneling electrons exert torques on the localized spin $\mathbf{S}$ which lead to corrections to the spin dynamics.[27] To lowest order in T_1, however, such effects are not present. Similarly, in what follows, we ignore the spin-flip interactions between the local moment and electrons in the substrate (i.e. we assume that the experimental temperature is higher than any relevant Kondo temperature ($T > T_K$)). Below the Kondo temperature, we may not ignore the spin-flip interactions of the localized spin with the substrate electrons- the local spin susceptibility will be heavily influenced by these interactions. Here we will only consider $T > T_K$ (a free impurity spin) for the sake of simplicity. For temperatures lower than the Kondo scale, the Kondo effect might manifest itself through interesting changes in the observed current noise that we discuss here for the free spin case. We now employ the Heisenberg representation and absorb the time dependence in all operators $\{\hat{O}\}$, i.e. $\hat{O}(t) = \exp[iHt]\hat{O}_S \exp[-iHt]$, with $\hat{O}_S = \hat{O}(t=0)$ the operator in the Schroedinger representation which we now forsake. All finite temperature expectation values $\langle\hat{O}(t)\rangle$ represent $\sum_i p_i \langle\psi_i(0)|\hat{O}(t)|\psi_i(0)\rangle$ with $\psi_i(t=0)$ the zero time wavefunction of the Schroedinger representation which does not evolve within the Heisenberg formulation and p_i its probability within the density matrix formulation. Let us now give a simple qualitative description of the effect that we address here. By directly computing dN_L/dt , the charge current

$$\hat{I}(t) = -ie \sum_{nn'\alpha\beta} c^{\dagger}_{Ln\alpha}(t)[T_0\delta_{\alpha\beta} + T_1 \mathbf{S}(t)\cdot\sigma_{\alpha\beta}]c_{Rn'\beta}(t) + h.c., \tag{31}$$

with e the electronic charge. The tunneling current has a part that depends on the localized spin via

$$\delta\hat{I}(t) = eT_1 \mathbf{S}(t)\cdot\mathbf{I}_{spin}(t), \tag{32}$$

where

$$\hat{\mathbf{I}}_{spin}(t) = -i \sum_{nn'\alpha\beta} c^{\dagger}_{Ln\alpha}(t)\hat{\sigma}_{\alpha\beta}c_{Rn'\beta}(t) + h.c., \tag{33}$$

is the spin polarization dependent contribution to the electronic current. This expression has a very transparent meaning. Its z-component, $\hat{I}^z_{spin}(t) = -i(c^{\dagger}_{L,\uparrow}c_{R,\uparrow} - c^{\dagger}_{L,\downarrow}c_{R,\downarrow}) + h.c.$, is the net flow of up spin minus the flow of down spin. A DC current of polarized electrons flowing from the tip to the surface trivially leads to a uniform spin polarized current $\hat{\mathbf{I}}_{spin}$. We assume that there is a non-vanishing *steady* spin polarized current component tunneling from the tip to the surface, assumed to be aligned along (or defining) the z axis: $\langle \hat{I}^i_{spin}(t)\rangle = \delta_{i,z}A^{\frac{1}{2}}$ + time dependent fluctuations, with a finite $A \neq 0$. An application of the diagrammatic analysis introduced in,[28] reveals that four contributions result each of which is, at most, of the order of the contribution that we discuss below. To lowest order in the hopping amplitude t_1, the electronic current-current correlation function originating from the spin dependent part that we wish to probe,

$$\langle [\delta\hat{I}(t), \delta\hat{I}(t')]_+\rangle = e^2T_1^2\langle S^i(t)S^j(t')\rangle\langle \hat{I}^i_{spin}(t)\hat{I}^j_{spin}(t')\rangle + (t \leftrightarrow t'), \tag{34}$$

where $i, j = x, y, z$ denote the spin components. To lowest non-trivial order in t_1, we treat the two temporal correlation functions $\chi(t-t') = \langle S^z(t)S^z(t')\rangle$ and $C(t-t') = \langle \hat{I}^i_{spin}(t)\hat{I}^j_{spin}(t')\rangle \to \langle \hat{I}^i_{spin}(t)\rangle\langle \hat{I}^j_{spin}(t')\rangle = \delta_{i,z}\delta_{j,z}A$ (for $|t-t'| \to \infty$) independently. To this order, the wavefunctions with respect to which we compute the expectation values are the products describing the decoupled evolution of both the spin and of the left and right contacts separately. When Fourier transformed, the symmetrized correlator $\langle [\delta\hat{I}(t), \delta\hat{I}(t')]_+\rangle$ is the current noise originating from the local spin. For small $(T_1/T_0) \ll 1$ (the experimental situation), $\mathcal{O}(\langle [\delta\hat{I}(t), \delta\hat{I}(t')]_+\rangle) = (T_1/T_0)^2I_0^2$. In evaluating the spin current correlator $C(t)$, we ignore the fluctuating contributions present for short times (large frequencies). The spin current correlator $C(t)$ has a finite, asymptotic, long time value, A, that reflects the spin polarized DC current emanating from the STM tip. In Fourier space, the current power spectrum is a convolution of the spectra associated with $\mathbf{S}$ (i.e. $\chi(\omega)$) and σ (the spin current correlator $C(\omega)$):

$$\langle |\delta\hat{I}(\omega)|^2\rangle = e^2T_1^2 \int \frac{d\omega_1}{2\pi}\chi(\omega_1)C(\omega - \omega_1) + (\omega \to -\omega). \tag{35}$$

At low frequencies, $C(\omega) \simeq 2\pi A\delta(\omega)$, and, consequently,

$$\langle |\delta\hat{I}(\omega)|^2\rangle = 2Ae^2T_1^2\chi(\omega) + ... \tag{36}$$

The ellipsis in Eq.(36) refer to the contribution to the convolution of Eq.(35) from the finite frequency (short time) contributions to $C(t)$. Assuming such finite frequency contributions in $C(\omega)$ have low spectral weight, the effect of these contributions will be low. This low order result is augmented by higher order corrections in T_1 as well as contributions arising from the connected component of the current current correlator which amounts to a shot noise like contribution. As noted, in Eq.(36) we neglected the effect of finite frequency components of $C(\omega)$ in the convolution of Eq.(35). We believe the large finite frequency components of the spin current $C(\omega)$ to be small as these correspond to transient fluctuations about an assumed steady state. This assumption is not necessary, however. More generally, we may deal with the full convolution in Eq.(35) directly without invoking any assumptions. We may potentially do this by first performing a measurement on a reference state. For instance, if we initially replace the single spin by a large cluster of a large fixed spin, we may then experimentally measure the resulting spin current $C(\omega)$. Armed with the knowledge of the spin current (from this earlier measurement on the magnetic cluster), once the noise spectrum $\langle |I(\omega)|^2\rangle$ is measured for the single spin, we can directly deconvolve Eq.(35) to obtain the spin susceptibility. Eqs.(35, 36) are the central result of this section. They vividly illustrate how the spectroscopy of the *noise* in the tunneling current $\langle |\delta I(\omega)|^2\rangle$ allows us to directly probe the spectrum of spin fluctuations encapsulated in $\chi(\omega)$. The spin polarized tunneling current provides a reference frame with respect to which we may measure the fluctuations of the localized spin $\mathbf{S}(t)$.

4.2. The origin of Spin Dependent Tunneling

We now elaborate on the origin and magnitude of the spin dependent tunneling matrix elements of Eq.(30). Their origin here is similar to that in earlier sections. The spin dependence of the tunneling originates from

the direct exchange dependence of the tunneling barrier.[25] The overlap of the electronic wave functions of the tip and surface, separated by a distance d is exponentially small and is given by a *spin dependent* tunneling matrix,$\hat{T} = \gamma \exp[-\sqrt{\frac{\Phi - J\mathbf{S}(t)\cdot\sigma}{\Phi_0}}]$, where we explicitly include the direct exchange between tunneling electron spin σ and the local spin $\mathbf{S}$. Here, J is the exchange interaction between the electrons tunneling from the tip and the local precessing spin $\mathbf{S}$. In the above, $\hat{T}$ is to be understood as a matrix in the internal spin indices, and Φ is the tunneling barrier height. Typically, Φ is a few eV. As a canonical value we may assume $\Phi = 4eV$, $\Phi_0 = \frac{\hbar^2}{8md^2}$ is related to the distance d between the tip and the surface.[29] As the exchange term in the exponent is small compared to the barrier height, we may expand the exponent in JS. Explicitly, $\hat{T}$ may be written as $\hat{T} = T_0 + T_1 \sigma \cdot \mathbf{S}(\mathbf{t})$ where,

$$T_0 = \gamma \exp(-(\Phi/\Phi_0)^{1/2}) \cosh[\frac{JS}{2\Phi}\sqrt{\frac{\Phi}{\Phi_0}}], \quad T_1 = \gamma \exp(-(\Phi/\Phi_0)^{1/2}) \sinh[\frac{JS}{2\Phi}\sqrt{\frac{\Phi}{\Phi_0}}] \tag{37}$$

for the spin independent and spin dependent tunneling respectively. As a typical rule of thumb, $T_1/T_0 \simeq \frac{JS}{2\Phi} \ll 1$.

4.3. Backaction effect of the tunneling current on the spin

We may use the tunneling Hamiltonian of Eq.(30) to estimate the decay rate of the localized spin state resulting from the spin scattering interaction associated with T_1. To second order this calculation is equivalent to a simple application Fermi's golden rule leading to an up-down spin flip rate $\frac{1}{\tau_s} = \pi T_1^2 N_L N_R eV$, with V is the voltage applied between the left and right electrodes. Similarly, the DC tunneling current I_0 is given by the tunneling rate of conduction electrons $\frac{1}{\tau_e} = \pi T_0^2 N_L N_R eV$, where $N_{L,R}$ denotes the density of states at the Fermi level of the tip and surface respectively.[30] Diagrammatically, both the spin scattering and electronic scattering rates arise from the simple bubble diagram whose real-time propagators are $G_L(t)$ and $G_R(-t)$, where $G_{L,R}$ correspond to the left and right Green's functions for the conduction electrons respectively. The sole difference between the two (spin dependent/independent) scattering rates is encapsulated in the prefactors. In the spin dependent scattering case (τ_s^{-1}) the raw value of the single loop integral appearing in the bubble diagram needs to be scaled by T_1^2. The spin independent scattering rate (τ_e^{-1}) is the much same albeit a scaling by the spin independent scattering amplitude squared (T_0^2). Comparing these simple results, we find

$$\frac{1}{\tau_s} = (\frac{T_1}{T_0})^2 \frac{1}{\tau_e} \simeq (\frac{JS}{2\Phi})^2 \frac{1}{\tau_e}. \tag{38}$$

The important outcome of this analysis is that the current induced broadening predicts a spin relaxation rate $\frac{1}{\tau_s} \propto I_0$ which may be experimentally tested. This result has a very simple interpretation: the impinging foreign electron tunneling rate for a DC current of magnitude $I_0 = 1nA$ is given by $\frac{1}{\tau_e} \sim 10^{10} Hz$. By contrast, the probability to produce a spin flip, sparked by the tunneling electrons, is proportional to T_1^2, which leads to Eqn.(38) for the linewidth. The full intrinsic line width is further enhanced by the coupling of the spin to the environment (e.g. the interaction between the spin and various substrate excitations) which may indeed further increase the spin flip rate. The net observed linewidth,

$$(T^*)^{-1} \simeq \tau_s^{-1} + \tau_{env}^{-1}, \tag{39}$$

includes both backaction contributions (τ_s^{-1}) and the aforementioned linewidth broadening due to coupling to the environment (τ_{env}^{-1}). The inverse backaction relaxation time scale sets a lower bound on the net relaxational linewidth of the single impurity spin. Given the typical values of the parameters in Eqn.(38), we estimate $\frac{1}{\tau_s} \sim 5 \times 10^6 Hz$ for our DC current of $I_0 \sim 1nA$, $J \sim 1$ eV, $\Phi \sim 4$ eV, and $S = 1/2$. Future experiments will help to clarify the linewidth dependence on the various parameters.

4.4. A Sizable Signal to Noise Ratio

We now demonstrate that the (signal to noise) ratio of $|\delta(\omega \to 0)|^2$ (the excess noise induced by the impurity spin) to $|I_{shot}(\omega \to 0)|^2$ (the shot noise already present in the absence of the impurity spin) can be of quite significant (of order unity). The finite frequency ratio $|\delta I(\omega)|^2/|I_{shot}(\omega)|^2$ was computed in a multitude of systems and shown

to be bounded by 4 or other numbers of order unity. By contrast, the low or zero frequency signal to noise ratio $|\delta I(\omega \to 0)|^2/|I_{shot}(\omega \to 0)|^2$ was found to be unbounded in many instances. For one calculation amogst many others demonstrating this explicitly, see e.g..[31] Nevertheless, as we highlight below, the low frequency signal to noise ratio, $|\delta I(\omega \to 0)|^2/|I_{shot}(\omega \to 0)|^2$, in our system is stringently bounded from above by a number of order unity, just as it is in many finite frequency situations. By considering typical values, we show that this ratio may saturate this upper bound and be markedly large, potentially allowing for single spin dynamics detection. To estimate this ratio, we note that $\langle \delta \hat{I}(t) \rangle = eT_1 \langle S^i(t) \hat{I}^i_{spin}(t) \rangle$ leading to $\mathcal{O}(eT_1 A^{1/2} \langle S^z(t) \rangle)$. As throughout, $\hbar = 1$, and spin is dimensionless. To obtain estimates of orders of magnitude let us inspect Eqs.(31, 33). The net electronic current I_e of Eq.(31) is of the order of I_0. Insofar as orders of magnitude are concerned, the spin current (I_{spin}) defined in Eq.(33) satisfies $\mathcal{O}(A^{1/2}) = \mathcal{O}(I_{spin}) = \mathcal{O}(\frac{I_e}{eT_0}) = \mathcal{O}(\frac{I_0}{eT_0})$. The shot noise, $\langle I^2_{shot} \rangle = aeI_0$, where the numerical constant $a = \mathcal{O}(1)$. Noting that $I_0 = \frac{e}{\tau_e}$, and making use of Eq.(36), the signal to noise ratio is found to be $\frac{\langle |\delta \hat{I}(\omega)|^2 \rangle}{\langle |\delta I_{shot}(\omega \to 0)|^2 \rangle} \sim \frac{T_1^2}{T_0^2} \chi(\omega) \frac{1}{\tau_e}$. The ratio $(T_1/T_0) \simeq \frac{J}{2\Phi}$. Inserting $\chi(\omega) = \langle \mathbf{S}_\omega \cdot \mathbf{S}_{-\omega} \rangle = \frac{1/T^*}{\omega^2 + 1/T^{*2}}$ for the suceptibility, we obtain

$$\frac{\langle |\delta I(\omega \to 0)|^2 \rangle}{\langle |\delta I_{shot}(\omega \to 0)|^2 \rangle} \sim \frac{T^*}{\tau_e} (\frac{T_1}{T_0})^2 \sim (\frac{J}{2\Phi})^2 \frac{T^*}{\tau_e}. \tag{40}$$

Inserting typical values, $J \simeq 0.1 - 1$ eV, $\Phi \simeq 4$ eV, $T^* \sim 10^{-8} - 10^{-6}$ seconds, and $\tau_e \sim 10^{-10}$ seconds (1nA), we find the above signal to noise ratio is, naively, 1-100. As promised, we now demonstrate, that within this allowed empirical regime, the signal to noise ratio will typically veer towards the lower end of the spectrum (i.e. may be of order unity at most). The bottleneck in the signal to noise ratio is set by the backaction effect of the single spin on the tunneling current. More explicitly, fusing Eqs.(38,39) together,

$$(T^*)^{-1} \simeq \tau_s^{-1} + \tau_{env}^{-1} \simeq (\frac{JS}{2\Phi})^2 \frac{1}{\tau_e} + \tau_{env}^{-1}, \tag{41}$$

leading us to conclude that T^* is less than or approximately equal to $(\frac{2\Phi}{JS})^2 \tau_e$. Inserting this in Eq.(40),

$$\frac{\langle |\delta I(\omega \to 0)|^2 \rangle}{\langle |\delta I_{shot}(\omega \to 0)|^2 \rangle} < (\frac{J}{2\Phi})^2 \frac{T^*}{\tau_e} < \mathcal{O}(1). \tag{42}$$

In the above equation, the inequalities may be approximately saturated. As the generic signal to noise ratio is bounded both from below and above by a number of order unity, the signal may indeed be quite sizable (of the order of the shot noise) and may be detected. This sizable ratio offers promise for such a detection.

5. CONCLUSIONS

We investigated spins embedded in various junctions leading to measurable effects. Are major findings are that:

(i) Inserting a spin into a normal junction immersed in a weak magnetic field leads to a modulation of the tunneling conductance. We predict the existence of a new mode whose frequency is double the Larmor frequency.

(ii) The tunneling current may, in turn, also alter the spin dynamics. This was made evident by the investigation of spin motion when embedded in Josephson junctions subjected to weak external magnetic fields. We predict spins to exhibit new nutations (*Josephson nutations*) as a consequence of pairing correlations. Our predicted effect is within possible reach of a proposed experiment.

(iii) We advanced noise spectroscopy as a new tool to probe single spin dynamics. Specifically, we investigated a single spin in embedded in an STM- substrate junction and illustrated how the noise in the current may allow us to discern the highly fluctuating single spin motion where other methods fail.

ACKNOWLEDGMENTS

We gratefully acknowledge A. Shnirman. This work was supported by the US DOE under LDRD X1WX and by NSF EIA-0205641 (MFC).

REFERENCES

1. M. Farle, "Ferromagnetic resonance of ultrathin metallic layers," *Rep. Prog. Phys.* **61**, p. 755, 1998.
2. R. Wiesendanger et al., "Topographic and magnetic-sensitive scanning tunneling microscope study of magnetite," *Science* **255**, p. 583, 1992.
3. G. A. Prinz, "Magnetoelectronics," *Science* **282**, p. 1488, 1998.
4. S. A. Wolf, "Spintronics: A spin-based electronics vision for the future," *Science* **294**, p. 1488, 2001.
5. B. E. Kane, "A silicon-based nuclear spin quantum computer," *Nature* **393**, p. 133, 1998.
6. D. Loss and D. P. DiVincenzo, "Quantum computation with quantum dots," *Phys. Rev. A* **57**, p. 120, 1998.
7. K. J. Bruland et al., "Force-detected magnetic resonance in a field gradient of 250 000 tesla per meter," *Appl. Phys. Lett.* **73**, p. 3159, 1998.
8. Y. Manassen, I. Mukhopadhyay and N. R. Rao, "Electron-spin-resonance stm on iron atoms in silicon," *Phys. Rev. B* **61**, p. 16223, 2000.
9. C. Durkan and M. E. Welland, "Electronic spin detection in molecules using scanning-tunneling- microscopy-assisted electron-spin resonance," *Appl. Phys. Lett.* **80**, p. 458, 2002.
10. A. V. Balatsky and I. Martin, "Theory of single spin detection with stm," *Quan. Inform. Process.* **1**, p. 53, 2002.
11. M. Buttiker, "Four-terminal phase-coherent conductance," *Phys. Rev. Lett.* **57**, p. 1761, 1986.
12. R. Landauer, "Electrical resistance of disordered one-dimensional lattices," *Philos. Mag.* **21**, p. 863, 1970.
13. Y. Meir and N. S. Wingreen, "Landauer formula for the current through an interacting electron region," *Phys. Rev. Lett.* **68**, p. 2512, 1992.
14. V. Ambegaokar and A. Baratoff, "Tunneling between superconductors," *Phys. Rev. Lett.* **10**, p. 486, 1963.
15. M. Sigrist and K. Ueda, "Phenomenological theory of unconventional superconductivity," *Rev. Mod. Phys.* **63**, p. 239, 1991.
16. J.-X. Zhu and A. V. Balatsky, "Josephson current in the presence of a precessing spin," *Phys. Rev. B* **67**, p. 174505, 2003.
17. G. S. U. Eckern and V. Ambegaokar, "Quantum dynamics of a superconducting tunnel junction," *Phys. Rev. B* **30**, p. 6419, 1984.
18. A. Larkin and Y. N. Ovchinnikov, "Decay of the supercurrent in tunnel junctions," *Phys. Rev. B* **28**, p. 6281, 1983.
19. E. Fradkin, *Field Theories of Condensed Matter Systems*, Addison-Wesley, Redwood City, 1991.
20. S. Sachdev, *Quantum Phase transitions*, Cambridge University Press, London, 1999.
21. J.-X. Zhu, Z. Nussinov, and A. V. Balatsky, "Vibration mode induced shapiro steps and backaction in josephson junctions," *arXiv.org* , pp. cond–mat/0306107, 2003.
22. L. Bulaevskii, M. Hruska, and G. Ortiz, "Tunneling measurement of quantum spin oscillations," *arXiv.org* , pp. cond–mat/0212049, 2002.
23. T. Sleator, E. L. Hahn, C. Hilbert, and J. Clarke, "Nuclear-spin noise," *Physical Review Letters* **55**, p. 1742, 1985.
24. E. B. Aleksandrov and V. S. Zapasskii *Sov. Phys. JETP* **54**, p. 64, 1981.
25. A. Balatsky, Y. Manassen, and R. Salem, "Esr-stm of a single precessing spin: Detection of exchange-based spin noise," *Phys. Rev. B* **82**, p. 1291, 2002.
26. A. Wachowiak et al., "Direct observation of internal spin structure of magnetic vortex cores," *Science* **298**, p. 577, 2002.
27. D. Ralph, "A new twist for magnets," *Science* **291**, p. 999, 2001.
28. A. Shnirman, D. Mozyrisky, and I. Martin, "Output spectrum of a measuring device at arbitrary voltage and temperature," *arXiv.org* , pp. cond–mat/0211618, 2002.
29. J. Tersoff and N. D. Lang, "Theory of scanning tunneling microscopy," *Methods of Experimental Physics* **27**, p. 1, 1993.
30. A. N. Korotkov, D. V. Averin, and K. K. Likharev, "Statistical properties of continuous-wave bloch oscillations in double-well semiconductor heterostructures," *Phys. Rev. B* **49**, p. 7548, 1994.
31. Y. Makhlin, G. Schon, and A. Shnirman, "Statistics and noise in a quantum measurement process," *Phys. Rev. Lett.* **85**, p. 4578, 2000.